Electronic Supplementary Material (ESI) for CrystEngComm.

Electronic Supplementary Information

for

(Isocyano group)···Lone Pair Interactions involving Coordinated Isocyanides: Experimental, Theoretical and CSD study

Alexander S. Mikherdov,* Svetlana A. Katkova, Alexander S. Novikov,* Maria M. Efremova, Elena Yu. Reutskaya, Mikhail A. Kinzhalov*

Saint Petersburg State University, Universitetskaya Nab., 7/9, Saint Petersburg, Russian Federation

E-mails: a.mikherdov@spbu.ru, a.s.novikov@spbu.ru, m.kinzhalov@spbu.ru

Table of Contents

S1. Materials and Instrumentation

Solvents, $PdCl_2$, CNXyl obtained from commercial sources and used as received (Sigma-Aldrich, St. Louis, MO, USA). The complexes *cis*-$[PdCl_2(CNXyl)_2]$ (**1**)[1] and 5-iodo-2,6-dimethylpyrimidin-4-amine[2] were prepared by the reported procedures. Mass-spectra were acquired on Bruker micrOTOF spectrometer (BRUKER Corporation, Billerica, MA, USA) equipped with ESI source; a CH_2Cl_2/MeOH mixture was used as the solvent. The instrument was operated at positive ion mode using *m/z* range of 50–3000. The capillary voltage of the ion source was set at –4500 V (ESI^+) and the capillary exit at +(70–150) V. The nebulizer gas pressure was 0.4 bar and drying gas flow was 4.0 L/min. The most intensive peak in the isotopic pattern is reported. IR spectra were measured on Shimadzu IRAffinity-1S FTIR instrument (Shimadzu Corporation, Kyoto, Japan) in KBr pellets (4000–400 cm^{-1}, resolution 2 cm^{-1}). The solid-state NMR experiment was performed on a Bruker Avance III NMR 400 WB spectrometer operating at 9.4 T. The CP/MAS NMR spectrum was acquired using a double-resonance 4 mm MAS Bruker probe at a resonance frequency of 162 MHz under 15 kHz MAS. The CP contact time was 3.5 μs with a delay between acquisitions of 2 sec.

S2. Synthetic work

Synthesis of 1. The mixture of palladium(II) isocyanide complex (50 mg, 0.114 mmol**)** and 5-iodo-2,6-dimethylpyrimidin-4-amine (57 mg, 0.228 mmol) in $C_2H_4Cl_2$ (3 mL) was refluxed for 24 h. After cooling the reaction mixture the final product was precipitated by addition of 5 ml of THF. Then crude product was filtered, washed with Et_2O (two 2-mL portions) and dried in air at RT. The pure complex was obtained as yellow solid and characterized by HR ESI-MS, FTIR, and ^{13}C- CP/MAS NMR spectroscopies.

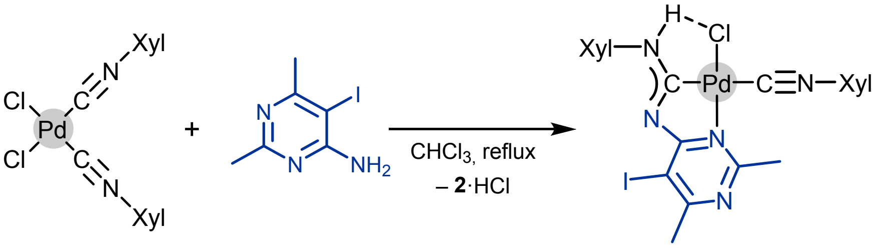

Scheme S1. Generation of trans-[PdCl(CNXyl)ACD] (**1**).

Yield is 35 mg (47%). Anal. Calcd. for $(C_{24}H_{25}N_5ClIPd)\cdot(C_2H_4Cl_2)_{1.5}$: C, 40.50; H, 3.90; N, 8.75, found: C, 40.37; H, 3.88; N, 9.03. HRESI$^+$-MS, *m/z*: calcd. for $C_{24}H_{25}ClN_5IPdH^+$ 653.9954, found 653.9945 $[M + H]^+$. IR (KBr, selected bands, cm^{-1}): 2198 (s) ν(N≡C). ^{13}C CP/MAS NMR: 19 (br.), 29(br.), 128 (br.), 136 (br.), 168.

S3. X-ray diffraction studies

The crystal of **1** was obtained in the reaction mixture. A single-crystal X-ray diffraction (SC-XRD) experiment was carried out using Xcalibur, Eos diffractometer (Agilent Technologies, Santa Clara, California, USA) The crystal was kept 100(2) K during all data collection. Structures were solved by the direct methods and refined by means of the ShelXL[3] program, incorporated in the OLEX2 program package.[4] Empirical absorption correction was applied in CrysAlisPro (Agilent Technologies, 2012) program complex using spherical harmonics, implemented in SCALE3 ABSPACK scaling algorithm. The crystallographic details are summarized in **Table S1–4**. Supplementary crystallographic data for this paper have been deposited at Cambridge Crystallographic Data Centre (CCDC **1909291**) and can be obtained free of charge via www.ccdc.cam.ac.uk/data_request/cif.

Table S1. Crystal data and structure refinement for **1**

Identification code	1
CCDC code	**1909291**
Empirical formula	$C_{24}H_{25}ClIN_5Pd$
Formula weight	652.24
Temperature/K	100.01(10)
Crystal system	triclinic
Space group	P-1
a/Å	8.8377(6)
b/Å	11.5913(9)
c/Å	12.6874(11)
α/°	68.122(8)
β/°	86.872(7)
γ/°	80.728(6)
Volume/Å^3	1190.32(17)
Z	2
ρ_{calc}g/cm^3	1.820
μ/mm^{-1}	2.211
F(000)	640.0
Crystal size/mm^3	0.1 × 0.1 × 0.1
Radiation	MoKα (λ = 0.71073)
2Θ range for data collection/°	5.574 to 62.172
Index ranges	$-11 \le h \le 10$, $-16 \le k \le 12$, $-17 \le l \le 14$
Reflections collected	11601
Independent reflections	6611 [R_{int} = 0.0302, R_{sigma} = 0.0542]
Data/restraints/parameters	6611/0/295
Goodness-of-fit on F^2	1.035
Final R indexes [I>=2σ (I)]	R_1 = 0.0322, wR_2 = 0.0630
Final R indexes [all data]	R_1 = 0.0450, wR_2 = 0.0696
Largest diff. peak/hole / e Å^{-3}	0.69/-0.78

The complex molecule lies in one plane with exception of the Xyl group at the carbene fragment. The palladium center adopts a slightly distorted square-planar geometry where diaminocarbene and isocyanide ligands are located in *trans*-position. The fragment [Pd]–C≡N–C is slightly deviate from linearity (∠(Pd1–C1–N1) = 170.4(3)°; (∠(C1–N1–C2) = 174.9(3)°). The Pd–isocyanide and Pd-carbene bonds (*d*(Pd1–C1) = 1.990(3) Å; *d*(Pd1–C10) = 2.068(3) Å) are slightly longer than those in the relevant aryl palladium-isocyanide and carbene species. [5-9] The bond length of the coordinated CN group (1.155(5) Å) fall in the interval of 1.144−1.155 Å, that is typical range for the CN triple bonds in the related *trans*-isocyanide complexes. [6, 7]

Table S2. Bond lengths for **1**.

Atom	Atom	Length/Å	Atom	Atom	Length/Å
I001	C20	2.094(3)	C20	C21	1.371(4)
Pd1	Cl1	2.3191(8)	C22	C24	1.500(4)
Pd1	N4	2.068(2)	C21	C23	1.501(4)
Pd1	C1	2.059(3)	C4	C3	1.390(4)
Pd1	C10	1.990(3)	C4	C5	1.380(4)
N4	C19	1.386(3)	C11	C12	1.399(4)
N4	C22	1.339(4)	C11	C16	1.404(4)
N3	C19	1.343(4)	C7	C9	1.490(4)
N3	C10	1.328(3)	C7	C6	1.383(4)
N1	C2	1.409(4)	C12	C18	1.492(4)
N1	C1	1.156(4)	C12	C13	1.395(4)
N5	C22	1.337(4)	C3	C8	1.512(4)
N5	C21	1.349(4)	C5	C6	1.381(4)
N2	C10	1.325(4)	C13	C14	1.380(4)
N2	C11	1.437(3)	C17	C16	1.500(4)
C2	C7	1.408(4)	C16	C15	1.393(4)
C2	C3	1.384(4)	C14	C15	1.379(5)
C19	C20	1.420(4)			

Table S3. Bond angles for **1**.

Atom	**Atom**	**Atom**	**Angle/°**	**Atom**	**Atom**	**Atom**	**Angle/°**
N4	Pd1	Cl1	170.08(7)	N5	C22	N4	125.1(3)
C1	Pd1	Cl1	85.15(8)	N5	C22	C24	115.5(3)
C1	Pd1	N4	104.48(11)	N5	C21	C20	120.4(3)
C10	Pd1	Cl1	92.25(9)	N5	C21	C23	115.7(3)
C10	Pd1	N4	78.23(11)	C20	C21	C23	123.9(3)
C10	Pd1	C1	176.49(12)	C5	C4	C3	120.8(3)
C19	N4	Pd1	109.85(18)	C12	C11	N2	121.0(3)
C22	N4	Pd1	132.40(19)	C12	C11	C16	122.4(3)
C22	N4	C19	117.7(2)	C16	C11	N2	116.5(3)
C10	N3	C19	113.1(2)	C2	C7	C9	122.0(3)
C1	N1	C2	175.0(3)	C6	C7	C2	116.1(3)
C22	N5	C21	118.7(3)	C6	C7	C9	121.9(3)
C10	N2	C11	127.8(2)	C11	C12	C18	122.6(3)
C7	C2	N1	116.6(3)	C13	C12	C11	117.4(3)
C3	C2	N1	119.4(3)	C13	C12	C18	120.0(3)
C3	C2	C7	124.0(3)	C2	C3	C4	117.1(3)
N4	C19	C20	118.4(3)	C2	C3	C8	121.2(3)
N3	C19	N4	120.1(2)	C4	C3	C8	121.7(3)
N3	C19	C20	121.5(3)	C4	C5	C6	120.5(3)
N1	C1	Pd1	170.4(3)	C14	C13	C12	121.2(3)
C19	C20	I001	118.3(2)	C11	C16	C17	121.4(3)
C21	C20	I001	122.1(2)	C15	C16	C11	117.6(3)
C21	C20	C19	119.6(3)	C15	C16	C17	121.0(3)
N3	C10	Pd1	118.6(2)	C15	C14	C13	120.3(3)
N2	C10	Pd1	122.2(2)	C5	C6	C7	121.5(3)
N2	C10	N3	119.2(3)	C14	C15	C16	121.0(3)
N4	C22	C24	119.4(3)				

S4. Hirshfeld surface analysis

The Hirshfeld molecular surface was generated by CrystalExplorer 3.1 program [10, 11] based on the results of the X-ray study of **1**. The normalized contact distances, d_{norm} [12], based on Bondi's van der Waals radii[13], were mapped into the Hirshfeld surface. In the color scale, negative values of d_{norm} are visualized by the red color indicating contacts shorter than the sum of van der Waals radii. The white color denotes intermolecular distances close to van der Waals contacts with d_{norm} equal to zero. In turn, contacts longer than the sum of van der Waals radii with positive d_{norm} values are colored in blue.

The molecular Hirshfeld surface represents an area where molecules come into contacts, and its analysis gives the information about the contributions of various intermolecular interactions in the crystal packing. For the visualization, we have used a mapping of the normalized contact distance (d_{norm}); its negative value enables identification of molecular regions of substantial importance for detection of short contacts. **Figure S2** depicts the Hirshfeld molecular surface for **1**.

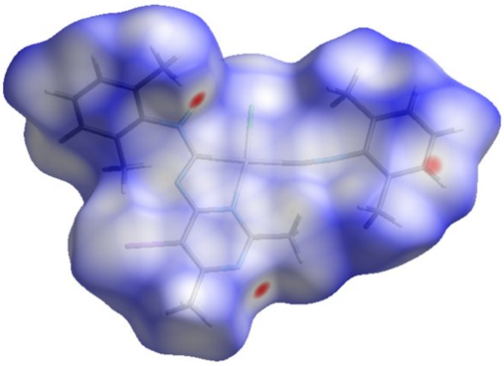

Figure S1. The Hirshfeld molecular surfaces for **1**. The regions of short intermolecular contacts visualized by red and white circle areas.

The Hirshfeld surface analysis for the XRD structure of **1** indicates the domination of the contacts involving hydrogen atoms, viz. H–H (50.5%), C–H (15.3%), I–H (7.3%), Cl–H (7.3%), N–H (6.2%). The X–H contacts provide the largest contributions to the molecular Hirshfeld surfaces because the fraction of these atoms is maximal. Apart from the contacts involving H atoms, the structure of **1** exhibits the C–C (4.7%) and N–C (2.2%) resembling to π-π stacking interactions and also less trivial I–C (1.5%) and Pd–C (1.1%) contacts. However, the Hirshfeld surface analysis does not answer the question of the energies of these contacts and, therefore, the DFT calculations needed to be further performed.

S5. Additional noncovalent interactions in crystal structure of 1

(Pyrimidin)···[Pd^{II}] interaction. The C···M distance in (pyrimidin)···[Pd^{II}] contact (3.555(3) Å) is larger than the sum of the corresponding Bondi vdW radii (3.33 Å), [13] but shorter than the sum of Alvarez vdW radii (3.92 Å).[14] In general, it is noteworthy that metals vdW radii cannot be precisely defined, and to date several values of vdW radii for Pd center based on different approaches are known, namely, varying from 1.63[13] and 2.15[14] Å. The corresponding angles between pyrimidine ring and palladium center (∠(N–C···Pd) = 86.5(2)º; ∠(C···Pd–C) = 88.2(1)º) are close to 90° indicating the interaction of *π*-system of pyrimidine with palladium center. The nature of such contact can be described as the resonance between three types of interactions, viz. πh···[M^{II}], dispersion, and semicoordination. The relevant type of metal···π interaction was reported by some of us for [M^{II}(Acac)$_2$] complexes (M = Pd, Pt, Cu).[15] The presence of this (pyrimidin)···[Pd^{II}] interaction was confirmed by DFT calculations followed by the topological analysis of the electron density distribution within the framework of Bader's theory (QTAIM method) (see **Table S4**).

N–H···Cl hydrogen bond. Additionally, the intramolecular N–H···Cl hydrogen bonding (HB) between NH-group of carbene fragment and chloride ligand at Pd^{II}-center was found. The distances between the heavy N2 and Cl1 atoms (3.038(3) Å) are substantially less than the sum of their Rowland (ΣvdW(N + Cl) = 3.40 Å) or Bondi (ΣvdW(N + Cl) = 3.30 Å) vdW radii, whereas the corresponding angle (132.7(2)°) is in the range 110−180°. Thus, this contact should be interpreted as HB according to the IUPAC criterion.[16]

S5. Processing of CSD

Processing of the Cambridge Structure Database (v 5.40) was performed using the ConQuest module (v 2.0.1). The analysis for the (isocyano group)···lp(X) (X = N, O, S, Se, F, Cl, Br, I without H atoms) interactions was based on three parameters, viz. distances C···X and N···X (d_1), and angles: N≡C···Hal and C≡N···Hal (a_1) (**Figure S2**, a). The distances were restricted by sum of Bondi vdW radii + 0.1 Å and a_1 angularity was set in range 0–180° for analysis of angular distribution. In case of several contacts, the shortest contact was selected.

For additional search for effect of external noncovalent contacts on the position of X in (isocyano group)···lp(X) interaction the additional parameters were introduced. In case of presence of hydrogen bonding the distance H···X (d_2) restricted by sum of Bondi vdW radii + 0.1 Å and a_2 angularity was set in range 110–180° (**Figure S2**, b). The analysis of external anion/lp···π interactions was carried out for contacts X···Y where Y is C or N atom with no or one H atom and connected to two non-H substituents (**Figure S2**, c). The distance Y···X (d_2) restricted by sum of Bondi vdW radii + 0.1 Å and $a_{2,3}$ angularity was set in range 65–115°.

Only structures with determined 3D geometries and with no error were included in the search query. In addition to this, powder structures were excluded from the search. To ensure that we have only high-quality structures, *R*-factor—which represents the agreement between the obtained crystallographic model and the experimental diffraction data—was kept below 0.1.

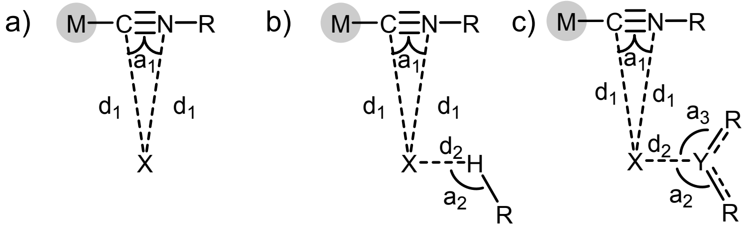

X = N, O, S, Se, F, Cl, Br, I without H atoms;
M = transition metals; R = Non H; Y = C, N with 0 or 1 H atoms

Figure S2. Parameters taken for processing CSD data.

S7. Computational details

All calculations have been carried out at the DFT level of theory with the help of the Gaussian-09[17] program package. The topological analysis of the electron density distribution with the help of the atoms in molecules (QTAIM) method developed by Bader[18] has been performed by using the Multiwfn program [19]. The electrostatic surface potential (ESP) was plotted using the Chemcraft program [http://www.chemcraftprog.com]. The Cartesian atomic coordinates for model structures are presented in the **Supplementary Files 2** (dimer of **1**), **3** ($ClAuCNCF_3$), and **4–7** ($ClAuCNCF_3$•Me_2O associates: gas phase optimized structure **4**, N···O contact fixed **5**, C···O contact fixed **6** and **7**).

For complex **1,** the QTAIM analysis was carried out for experimental XRD geometry of dimeric associate at the ωB97XD/x2c-TZVPPall and M06-2X/CEP-121G levels of theory, whereas ESP calculation have been performed for experimental XRD geometry of monomer of **1** at the M06-2X/CEP-121G level of theory. For $ClAuCNCF_3$•Me_2O associate and isolated $ClAuCNCF_3$ and Me_2O species, the full geometry optimization in gas phase following the QTAIM and NBO analyses and ESP calculations were carried out at the M06-2X/CEP-121G level of theory. No symmetry restrictions have been applied during the geometry optimization procedure. The Hessian matrices were calculated analytically in order to prove the location of correct minima on the potential energy surfaces (no imaginary frequencies).

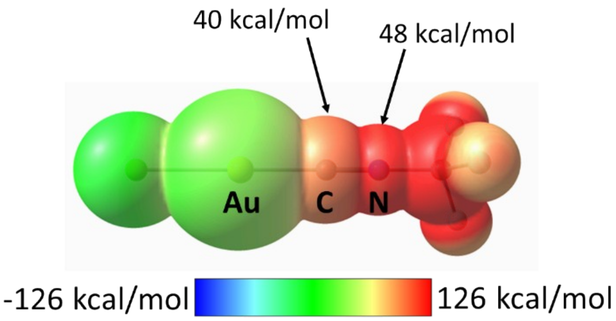

Figure S3. Distribution of electrostatic potential $V_S(\mathbf{r})$ calculated on the 0.001 a.u. molecular surface for $ClAuCNCF_3$.

Table S4. Values of the density of all electrons – $\rho(\mathbf{r})$, Laplacian of electron density – $\nabla^2\rho(\mathbf{r})$ and appropriate λ_2 eigenvalues, energy density – H_b, potential energy density – $V(\mathbf{r})$, and Lagrangian kinetic energy – $G(\mathbf{r})$ (a.u.) at the bond critical points (3, –1), corresponding to various noncovalent interactions in model supramolecular associates, bond lengths – l (Å), as well as energies for these contacts E_{int} (kcal/mol), defined by two approaches.*

Contact	$\rho(\mathbf{r})$	$\nabla^2\rho(\mathbf{r})$	λ_2	H_b	$V(\mathbf{r})$	$G(\mathbf{r})$	$E_{int}{}^a$	$E_{int}{}^b$	l
Dimer of **1**									
ωB97XD/x2c-TZVPPall level of theory									
N···I	0.007	0.020	-0.008	0.001	-0.003	0.004	0.9	1.1	3.687
Pd···C	0.006	0.016	-0.008	0.001	-0.003	0.003	0.9	0.8	3.555
M06-2X/CEP-121G level of theory									
N···I	0.006	0.021	-0.008	0.001	-0.003	0.004	0.9	1.1	3.687
Pd···C	0.006	0.018	-0.008	0.001	-0.003	0.004	0.9	1.1	3.555
$ClAuCNCF_3$•Me_2O associate (gas phase optimized geometry)									
N···O	0.015	0.075	-0.018	0.003	-0.012	0.015	3.8	4.0	2.724
F···O	0.010	0.044	0.013	0.002	-0.007	0.009	2.2	2.4	2.871
$ClAuCNCF_3$•Me_2O associate (N···O contact fixed)									
N···O	0.036	0.199	-0.040	0.002	-0.045	0.047	14.1	12.7	2.303
F8···C11	0.013	0.067	-0.020	0.003	-0.011	0.014	3.5	3.8	2.749
$ClAuCNCF_3$•Me_2O associate (C···O contact fixed)									
C···O	0.011	0.045	-0.014	0.002	-0.007	0.009	2.2	2.4	2.866
$ClAuCNCF_3$•Me_2O associate (C···O contact fixed)									
C···O	0.027	0.117	-0.033	0.003	-0.024	0.026	7.5	7.0	2.415

[*] The Poincare-Hopf relationship was satisfied during the topological analysis of the electron density distribution in all cases.

[a] $E_{int} = -V(\mathbf{r})/2$ [20]

[b] $E_{int} = 0.429G(\mathbf{r})$ [21]

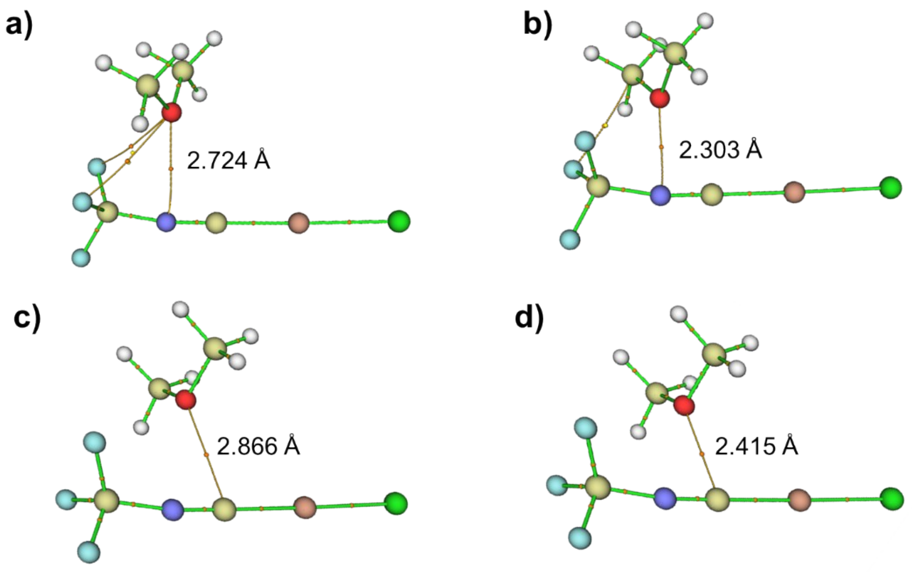

Figure S4. Molecular graphs from the QTAIM analysis of the $ClAuCNCF_3$•Me_2O associates: a) optimized gas phase geometry, b) optimized structure with fixed N···O contact, c) and d) optimized structures with fixed C···O contact. Bond critical points (3, −1) are shown in orange, ring critical points (3, +1) − in yellow. The Poincare-Hopf relationship was satisfied in all cases.

References

1. A. S. Mikherdov, M. A. Kinzhalov, A. S. Novikov, V. P. Boyarskiy, I. A. Boyarskaya, D. V. Dar'in, G. L. Starova and V. Y. Kukushkin, *J. Am. Chem. Soc.*, 2016, **138**, 14129-14137.
2. O. O. Orazi, R. A. Corral and H. E. Bertorello, *J. Org. Chem.*, 1965, **30**, 1101-1104.
3. G. M. Sheldrick, *Acta Crystallogr., Sect. C: Struct. Chem.*, 2015, **71**, 3–8.
4. O. V. Dolomanov, L. J. Bourhis, R. J. Gildea, J. A. K. Howard and H. Puschmann, *J. Appl. Cryst.*, 2009, **42**, 339–341.
5. S. A. Katkova, M. A. Kinzhalov, P. M. Tolstoy, A. S. Novikov, V. P. Boyarskiy, A. Y. Ananyan, P. V. Gushchin, M. Haukka, A. A. Zolotarev, A. Y. Ivanov, S. S. Zlotsky and V. Y. Kukushkin, *Organometallics*, 2017, **36**, 4145-4159.
6. M. A. Kinzhalov, K. V. Luzyanin, I. A. Boyarskaya, G. L. Starova and V. P. Boyarskiy, *J. Mol. Struct.*, 2014, **1068**, 222-227.
7. M. A. Kinzhalov, M. V. Kashina, A. S. Mikherdov, E. A. Mozheeva, A. S. Novikov, A. S. Smirnov, D. M. Ivanov, M. A. Kryukova, A. Y. Ivanov, S. N. Smirnov, V. Y. Kukushkin and K. V. Luzyanin, *Angew. Chem. Int. Ed.*, 2018, **57**, 12785-12789.
8. T. B. Anisimova, M. F. C. Guedes da Silva, V. Y. Kukushkin, A. J. L. Pombeiro and K. V. Luzyanin, *Dalton Trans.*, 2014, **43**, 15861-15871.
9. A. Tskhovrebov, K. Luzyanin, M. Kuznetsov, V. Sorokoumov, I. Balova, M. Haukka and V. Kukushkin, *Organometallics*, 2011, **30**, 863-874.
10. S. K. Wolff, D. J. Grimwood, J. J. McKinnon, M. J. Turner, D. Jayatilaka and M. A. Spackman, *CrystalExplorer, Version 3.1,* University of Western Australia,2012.
11. M. A. Spackman and D. Jayatilaka, *CrystEngComm*, 2009, **11**, 19-32.
12. J. J. McKinnon, D. Jayatilaka and M. A. Spackman, *Chem. Commun.*, 2007, **37**, 3814-3816.
13. A. Bondi, *J. Phys. Chem.*, 1964, **68**, 441-451.
14. S. Alvarez, *Dalton Trans.*, 2013, **42**, 8617-8636.
15. A. V. Rozhkov, A. S. Novikov, D. M. Ivanov, D. S. Bolotin, N. A. Bokach and V. Y. Kukushkin, *Cryst. Growth Des.*, 2018, **18**, 3626-3636.
16. E. Arunan, G. R. Desiraju, R. A. Klein, J. Sadlej, S. Scheiner, I. Alkorta, D. C. Clary, R. H. Crabtree, J. J. Dannenberg, P. Hobza, H. G. Kjaergaard, A. C. Legon, B. Mennucci and D. J. Nesbitt, *Pure Appl. Chem.*, 2011, **83**, 1637-1641.
17. M. J. Frisch, G. W. Trucks, H. B. Schlegel, G. E. Scuseria, M. A. Robb, J. R. Cheeseman, G. Scalmani, V. Barone, Mennucci, B., G. A. Petersson, H. Nakatsuji, M. Caricato, X. Li, H. Hratchian, P., A. F. Izmaylov, J. Bloino, G. Zheng, J. L. Sonnenberg, M. Hada, M. Ehara, K. Toyota, R. Fukuda, J. Hasegawa, M. Ishida, Nakajima, T., Y. Honda, O. Kitao, H. Nakai, T. Vreven, J. A. Montgomery, J. E. Peralta, F. Ogliaro, M. Bearpark, J. J. Heyd, E. Brothers, Kudin, K. N., V. N. Staroverov, R. Kobayashi, J. Normand, K. Raghavachari, A. Rendell, J. C. Burant, S. S. Iyengar, J. Tomasi, M. Cossi, Rega, N., J. M. Millam, M. Klene, J. E. Knox, J. B. Cross, V. Bakken, C. Adamo, J. Jaramillo, R. Gomperts, R. E. Stratmann, O. Yazyev, A. J. Austin, R. Cammi, C. Pomelli, J. W. Ochterski, R. L. Martin, K. Morokuma, V. G. Zakrzewski, G. A. Voth, P. Salvador, J. J. Dannenberg, S. Dapprich, A. D. Daniels, J. Farkas, Foresman, B., J. V. Ortiz, J. Cioslowski and D. J. Fox, *Gaussian 09*, Gaussian, Inc., Wallingford CT, 2010.
18. R. F. W. Bader, *Chem. Rev.*, 1991, **91**, 893-928.
19. T. Lu and F. W. Chen, *J. Comput. Chem.*, 2012, **33**, 580-592.
20. E. Espinosa, E. Molins and C. Lecomte, *Chem. Phys. Lett.*, 1998, **285**, 170-173.
21. M. V. Vener, A. N. Egorova, A. V. Churakov and V. G. Tsirelson, *J. Comput. Chem.*, 2012, **33**, 2303-2309.